ROYAL SOCIETY OF CHEMISTRY

PAPER

Check for updates

Implementation-focused evaluation of transmission low-frequency Raman spectroscopy parameters for non-destructive quality control of solid dosage forms

Reo Kasahara,†[a] Motoki Inoue [ID] *†[b] and Toshiro Fukami[a]

Transmission low-frequency Raman spectroscopy (TLRS) offers unique advantages for non-destructive characterization of crystalline phases in pharmaceutical solid dosage forms. While the analytical principle has been previously demonstrated, its practical implementation for routine quality control (QC) has not been systematically assessed. This study evaluates the effects of key formulation and measurement parameters—tablet thickness, compaction pressure, particle size, and laser power—on TLRS performance using intact amorphous carbamazepine tablets containing crystalline Form III. In transmission mode, spectral intensity peaked at an optimal thickness and decreased at higher compaction pressures, while smaller particle sizes provided more reproducible spectra and improved semi-quantitative accuracy. Principal component analysis (PCA) enabled clear discrimination and compositional ranking for low-level crystalline content (≥5%) across a 0–30% loading range. These findings provide practical insights into TLRS implementation and indicate its potential utility for future analytical applications.

Introduction

The complex molecular structures and physicochemical limitations of APIs make it challenging to improve their solubility and oral bioavailability.[1] Therefore, various strategies such as co-crystallization,[2–4] nanocrystallization,[5,6] and amorphization[7–9] have been actively explored. Among them, amorphization has garnered increasing interest owing to its ability to enhance apparent solubility and dissolution rates compared to crystalline formulations. However, the amorphous form is thermodynamically unstable and prone to recrystallization during storage, potentially impacting drug solubility and bioavailability.[10,11] Therefore, the detection and quantification of crystalline content in amorphous formulations are essential for formulation development and quality assurance.[12,13]

Conventional techniques for detecting residual crystallinity include powder X-ray diffraction (PXRD), solid-state nuclear magnetic resonance (ss-NMR), differential scanning calorimetry (DSC), near-infrared spectroscopy, and Raman spectroscopy.[14–16] Although PXRD is widely used and accessible, its sensitivity strongly depends on measurement con-

ditions. Under routine settings, a detection limit of approximately 10% is often cited.[14] However, optimized methods—such as those described by Chen *et al.*—have demonstrated detection thresholds as low as 1–2%.[17] This variability highlights the importance of experimental parameters and suggests that alternative, non-destructive methods may be more suitable for detecting low levels of crystallinity in intact dosage forms. Furthermore, ss-NMR requires long measurement times and complex instrumentation, while DSC often struggles with signal overlap in multicomponent systems. Most of these methods also involve destructive sample preparation, making them less ideal for tablet-level quality control.[18]

In contrast, Raman spectroscopy offers a nondestructive and rapid alternative with minimal sample preparation. Particularly, low-frequency Raman spectroscopy (LRS) in the 0–200 cm^{-1} range can provide vibrational information related to intermolecular lattice modes, which are highly sensitive to crystalline structures.[19–26] This spectral region facilitates a clear distinction between crystalline and amorphous materials, as well as the identification of trace crystalline phases within predominantly amorphous matrices.[27,28]

While backscattering is the most commonly used configuration for Raman measurements, it is limited by localized surface sampling, which can lead to poor reproducibility when analyzing inhomogeneous samples such as tablets.[29] Therefore, various averaging techniques have been explored, including multipoint acquisition,[30] rotation, and wide-area

[a] Meiji Pharmaceutical University, 2-522-1, Noshio, Kiyose, Tokyo 204-8588, Japan
[b] Hoshi University, 2-4-41, Ebara, Shinagawa-Ku, Tokyo 142-8501, Japan.
E-mail: inoue.motoki@hoshi.ac.jp
† These authors contributed equally.

sampling.[31,32] Among them, the transmission-mode Raman approach, which collects scattering from the backside of the sample, demonstrates superior depth penetration and quantitative performance.[33–38]

Although our previous study demonstrated the use of transmission-mode LRS for discriminating between crystalline polymorphs of carbamazepine, the present work addresses a fundamentally different analytical objective. Specifically, this study focuses on detecting and quantifying residual crystalline content embedded within an amorphous matrix—a challenge not addressed in our earlier work. This application of TLRS introduces new considerations related to signal sensitivity, sample heterogeneity, and multivariate spectral modeling.

Despite its advantages, transmission LRS (TLRS) has not been fully optimized for practical use. The effects of tablet thickness, compaction pressure, particle size, and laser intensity on signal sensitivity and spectral reproducibility remains unclear.[39,40] Therefore, in this study, we evaluated the feasibility and robustness of TLRS in detecting and quantifying trace crystalline content in amorphous tablets, using carbamazepine (CBZ) as a model drug. Through systematic investigation of key tablet manufacturing and measurement conditions, we aimed to establish practical guidelines for effectively implementing TLRS in pharmaceutical analysis.

Results

Effect of tablet mass (thickness) on Raman signal intensity

The impact of tablet mass, associated with tablet thickness, on Raman spectral intensity was investigated. Fig. 3 illustrates the relationship between peak intensity at 37 cm^{-1} and tablet thickness, as observed in both backscattering and transmission-mode measurements. Tablet mass was varied while
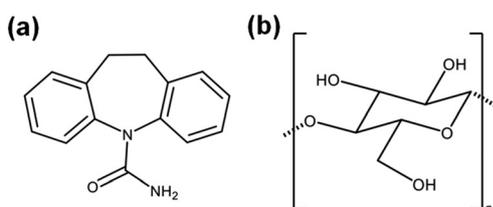

Fig. 1 Chemical structures of materials used in this study: (a) carbamazepine, (b) microcrystalline cellulose.
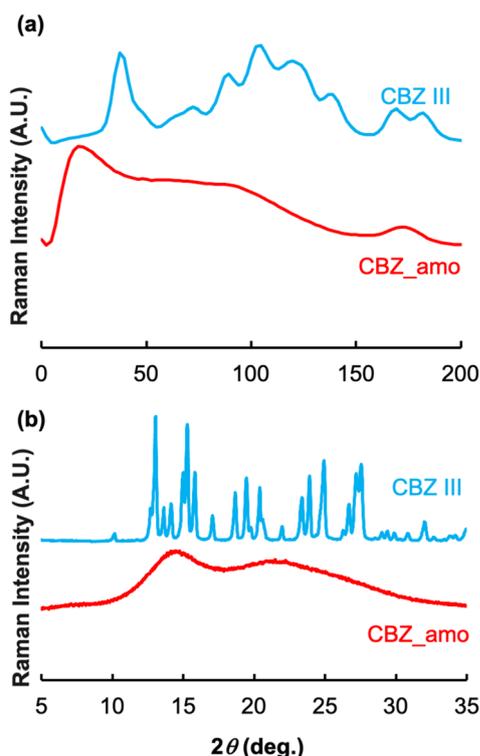

Fig. 2 (a) Low-frequency Raman spectral and (b) powder X-ray diffraction patterns of prepared samples, confirming amorphous and crystalline forms of carbamazepine.
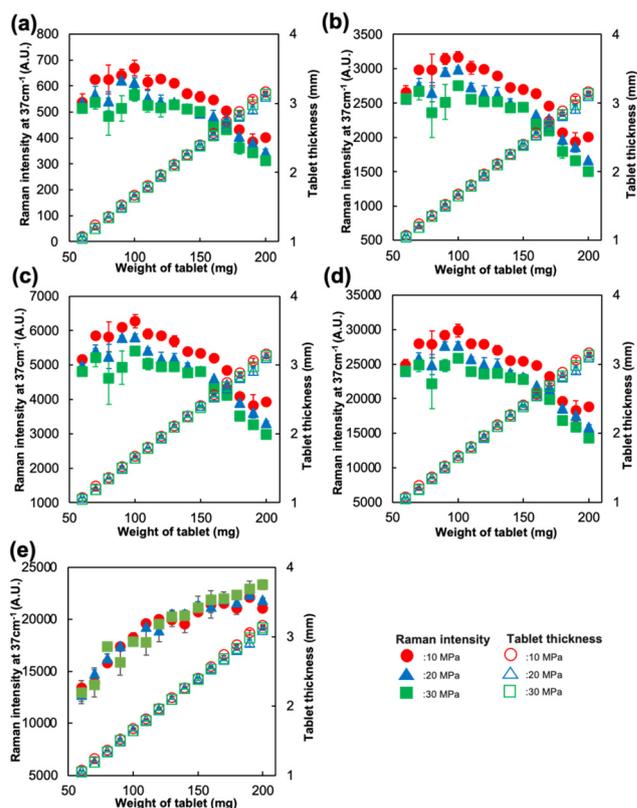

Fig. 3 Effect of tablet thickness on Raman spectral intensity measured at different exposure times ($N = 3$, error bars represent the standard deviation of three measurements). The left vertical axis represents Raman spectral intensity, the right vertical axis represents tablet thickness (mm), and the horizontal axis represents tablet pressure (MPa). ● : 10 MPa, ▲ : 20 MPa, and ■ : 30 MPa (hollow symbols represent tablet thickness). Tablets prepared at tablet pressures of 10, 20, and 30 MPa were used for (a) transmission measurement at 0.1 s, (b) transmission measurement at 0.5 s, (c) transmission measurement at 1 s, (d) transmission measurement at 5 s, and (e) backscattering measurement at 1 s.

maintaining compaction pressures of 10, 20, or 30 MPa. In transmission-mode spectra (Fig. 3a–d), signal intensity increased with tablet thickness up to approximately 100 mg, beyond which it gradually declined. This trend was consistent across all applied compaction pressures and exposure times. In contrast, backscattering-mode spectra (Fig. 3e) showed a steady increase in signal intensity with increasing tablet mass. The right *y*-axis of the graphs represents tablet thickness, whereas the left *y*-axis denotes Raman intensity. Although backscattering mode is surface-sensitive, the increased signal intensity can be attributed to several factors. While backscattering Raman spectroscopy primarily probes the tablet surface, the incident laser can penetrate a limited depth, generating scattering from subsurface layers. As tablet thickness increases, the effective sampling volume also increases, thereby enhancing the overall signal intensity. Additionally, thicker tablets may exhibit greater surface or crystallite density, further improving scattering efficiency. These combined effects likely account for the observed trend in Fig. 3(e).

Tablet compaction pressure

The effect of compaction pressure on spectral intensity was examined using tablets with varying mass and constant formulation composition. A slight reduction in tablet thickness was observed with increasing pressure. Higher compaction pressures tended to decrease the peak intensity in transmission-mode measurements, regardless of tablet mass (Fig. 4), suggesting that increasing density may hinder light penetration in transmission-mode detection.

Excitation laser intensity

The optimization of laser power is critical to balancing signal strength and thermal safety. Excessive laser intensity can cause sample degradation, while low intensity may yield insufficient signals. Spectral intensity increased with laser power up to 300 mW, which was the maximum output available with the current system (Fig. 5). Although higher laser powers were not evaluated, 300 mW yielded the strongest signal without signs of sample degradation. Therefore, this condition was selected for subsequent measurements. The term "optimal" is used here within the context of the available instrument parameters.

Particle size

To assess the impact of particle size on spectral intensity and quantification, tablets comprising different particle size fractions were analyzed. Tablets were prepared using 100 mg of powder at a compaction pressure of 10 MPa. Three particle size categories were examined: ≤100, 100–212, and >212 μm. Fig. 6 shows the spectral responses of tablets containing increasing proportions of CBZ Form III (0%–30%) blended with CBZ_amo. Additionally, amorphous-only samples produced broad, featureless spectra, whereas the incorporation of crystalline content resulted in distinct Form III-specific peaks. This trend was consistent across all particle sizes. Fig. 7 presents the quantitative relationship between particle size and
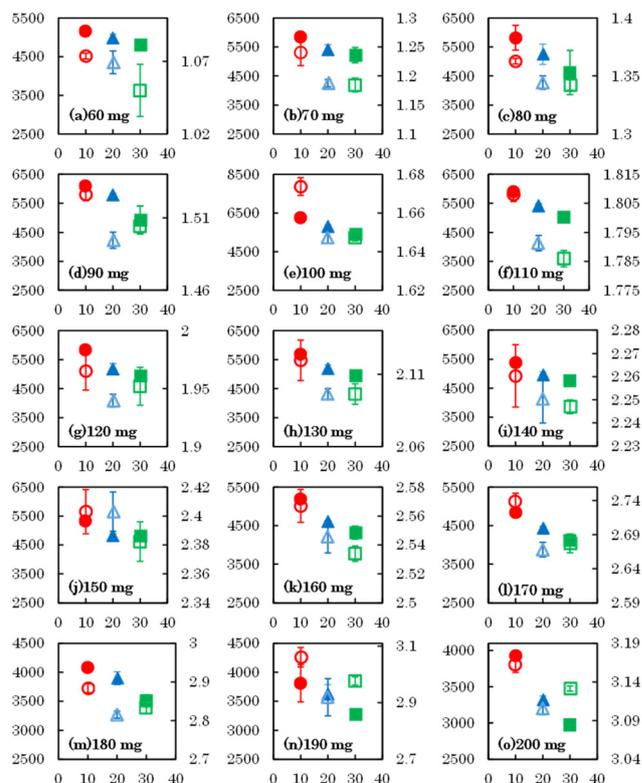

Fig. 4 Relationship between signal intensity and tablet thickness measured at an exposure time of 1 s, categorized by sample mass (*N* = 3, error bars represent the standard deviation of three measurements). The left vertical axis represents Raman spectral intensity, the right vertical axis represents tablet thickness (mm), and the horizontal axis represents tablet pressure (MPa). ● : 10 MPa, ▲ : 20 MPa, and ■ : 30 MPa (hollow symbols represent tablet thickness).
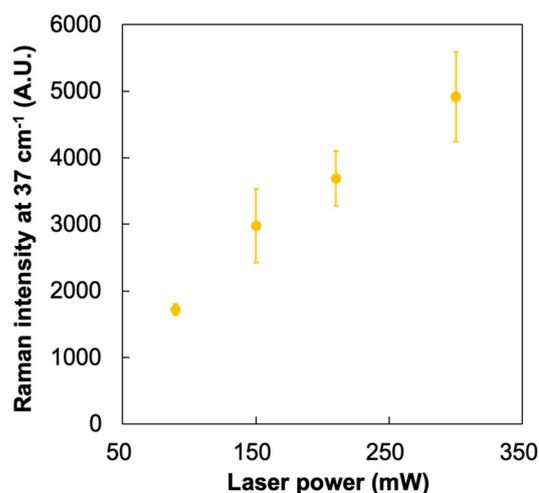

Fig. 5 Influence of excitation laser power on Raman spectral intensity. Signal intensities increased with laser power up to 300 mW, which was selected as the optimal condition for subsequent experiments (*N* = 3, error bars represent the standard deviation).
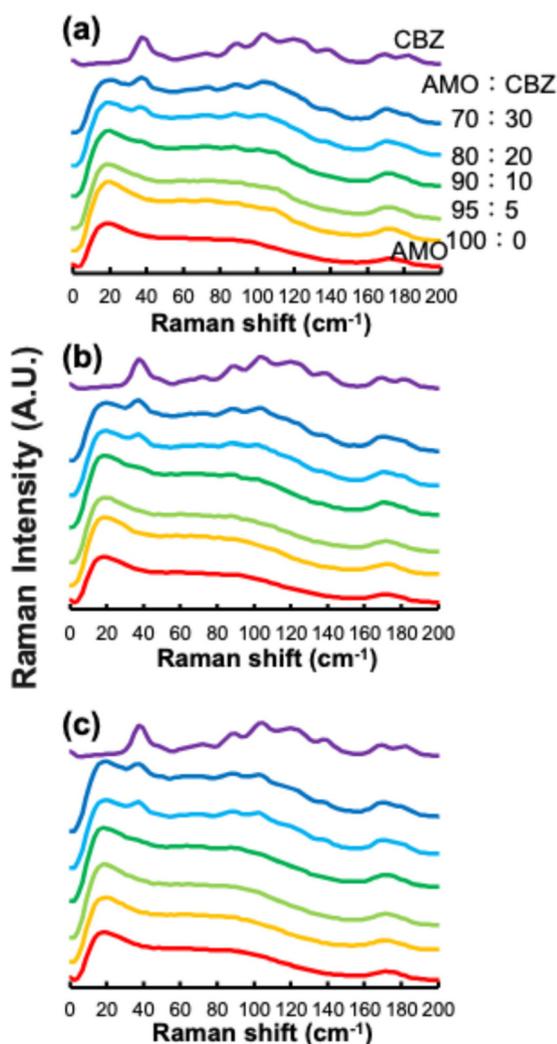
Fig. 6 Correlation between carbamazepine (CBZ) Form III concentration and Raman spectral intensity in CBZ_amo tablets at different particle size ranges: (a) ≤100 μm, (b) 100–212 μm, and (c) >212 μm. Increasing crystalline content led to distinct spectral peaks.

Fig. 7 Effect of particle size on Raman peak intensity at 37 cm^{-1} in tablets composed entirely of carbamazepine Form III (N = 3, error bars represent the standard deviation). Larger particles exhibited stronger but more variable signals, while smaller particles produced more consistent results.

CBZ_amo : Form III ratio, indicating effective separation. However, clustering was not observed for particles >212 μm. When the analysis range was expanded to 10–200 cm^{-1} (Fig. 8d–f), improved clustering was observed, even for the largest particle size group. These results suggest that expanding the analysis region enables the inclusion of multiple spectral features, thereby enhancing the differentiation of crystalline content, even in heterogeneous samples. Tablets prepared with smaller particles exhibited more distinct clustering, likely due to increased homogeneity and spectral averaging, consistent with previous findings.[40]

Discussion

In this study, we investigated the potential of TLRS for detecting and quantifying crystalline components embedded within amorphous pharmaceutical tablets. The results demonstrated that both formulation and measurement parameters significantly influenced the spectral intensity and quantification performance of TLRS. These parameters included tablet thickness, compaction pressure, and particle size.

Regarding tablet thickness, the conventional backscattering mode showed increased signal intensity with increasing thickness, consistent with prior findings that denser samples produce stronger surface scattering due to enhanced laser interaction with crystalline regions.[42] In contrast, the transmission mode exhibited a peak intensity at an optimal thickness (~1.76 mm), followed by a decline with increasing thickness. This phenomenon suggests that, beyond a certain thick-

peak intensity at 37 cm^{-1} for tablets composed entirely of CBZ Form III. Larger particle sizes yielded higher signal intensities but exhibited greater variability. Moreover, statistical analysis revealed significant differences ($p < 0.01$) between particle size groups.

Multivariate data analysis

PCA was conducted to evaluate whether differences in crystalline content could be represented using Raman spectral data alone. PCA is an unsupervised multivariate technique used to reduce the dimensionality of spectral datasets while retaining meaningful variation. Notably, particle size can significantly affect Raman spectral intensity.[41] In this study, we assessed how particle size influences quantitative discrimination via PCA. Fig. 8a–c shows PCA score plots using the 21–52 cm^{-1} spectral range. For particle sizes ≤100 and 100–212 μm, samples formed distinct clusters based on the
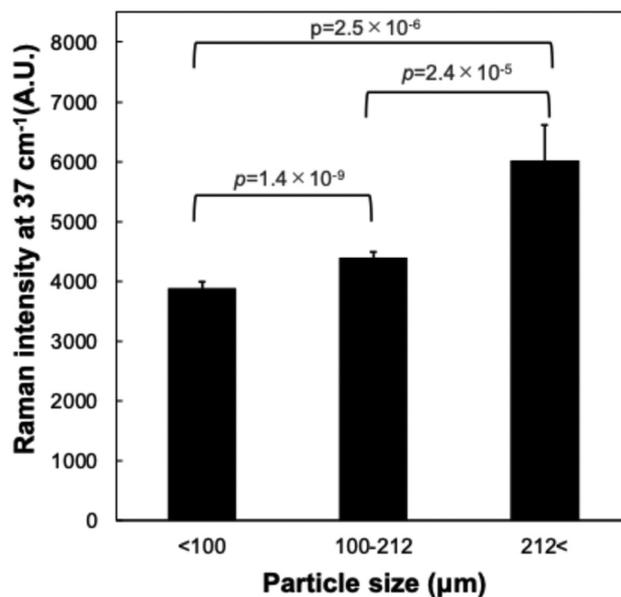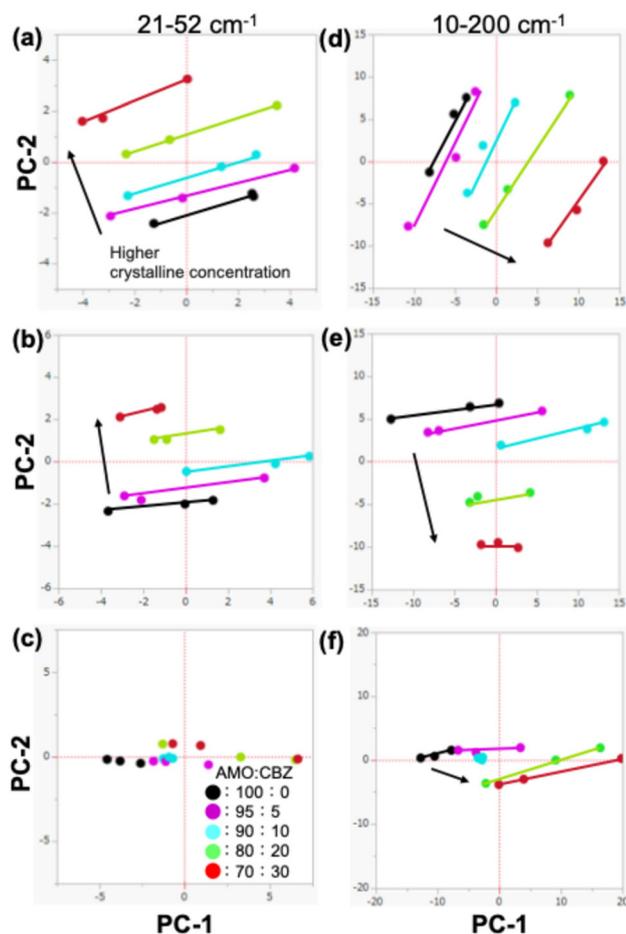
Fig. 8 Principal component analysis (PCA) score plots illustrating the impact of particle size and spectral range on sample clustering based on crystalline content. (a–c): PCA using the 21–52 cm^{-1} range; (d–f): PCA using the 10–200 cm^{-1} range. Particle size groups: (a and d) ≤100 µm, (b and e) 100–212 µm, and (c and f) >212 µm. CBZ_amo : the CBZ Form III ratio is represented by symbols: ● 100 : 0, ● 95 : 5, ● 90 : 10, ● 80 : 20, and ● 70 : 30. PC1 = x-axis; PC2 = y-axis.

ness, laser penetration and photon collection become less efficient, leading to a reduction in signal intensity.[37] This optimal thickness range closely corresponds to that of many commercially available pharmaceutical tablets, which are 2–4 mm. The fact that stable and reproducible TLRS spectra were obtained at this thickness supports the practical applicability of the method to real dosage forms. Additionally, compaction pressure had opposing effects on different detection modes. In the backscattering configuration, increasing compaction pressure enhanced signal intensity, likely due to increased tablet density and surface reflectance. However, in the transmission mode, the signal decreased with higher compaction pressures, likely because denser matrices attenuate light transmission and reduce subsurface scattering.[41] It should also be noted that the compaction conditions used in this study differ from those typically used in industrial tablet manufacturing. In practice, rotary presses apply pressure for only tens to hundreds of milliseconds, whereas our manual

press involved dwell times of several seconds. The compaction pressures (10–30 MPa) were selected not to mimic production conditions, but to produce tablets with sufficient mechanical strength and a range of densities suitable for systematic TLRS evaluation. These settings enabled us to investigate how compaction pressure affects light transmission and Raman signal quality under controlled conditions.

One notable advantage of transmission-mode low-frequency Raman spectroscopy (TLRS) is its ability to probe deeper regions of the tablet compared to conventional backscattering configurations. In this study, we confirmed that distinct Raman signals from crystalline carbamazepine were detectable even in tablets with a thickness of approximately 2–4 mm. This demonstrates that the 808 nm near-infrared laser employed in TLRS provides sufficient penetration depth to access internal layers that are typically inaccessible in backscattering mode. The laser traverses the entire tablet and the scattered light is collected from the opposite side, the resulting spectra represent bulk-averaged information with minimal surface bias. These features contribute to the improved reproducibility and quantification reliability observed in transmission-mode measurements. Particle size was found to be a critical factor affecting spectral variability and quantification. Tablets comprising smaller particles produced more reproducible spectra with lower measurement errors, owing to improved homogeneity in the sampling volume. This finding aligns with that of a previous study suggesting that finer particles enhance spectral averaging and signal consistency.[40] The quantification of CBZ Form III within the CBZ_amo matrix was also more accurate with smaller particles, supporting the importance of particle uniformity in TLRS-based measurements. In the multivariate analysis, PCA confirmed that the spectral differences associated with crystalline content could be effectively captured, especially in samples with smaller particles. When the particle size exceeded 212 µm, spectral clustering decreased unless the analysis range was extended to include broader frequency bands (10–200 cm^{-1}). This result highlights the efficacy of employing a broader spectral window to capture multiple lattice vibrational modes, thereby improving discrimination in samples with lower homogeneity.[40,41] Overall, the findings underscore that variations in tablet thickness, density, and particle size substantially affect TLRS performance. Therefore, standardizing tablet preparation conditions is essential for achieving reproducible and quantitative analysis. These results suggest that TLRS is feasible for detecting low levels of residual crystallinity in amorphous formulations, indicating its potential application in tablet quality evaluation. However, it should be noted that the present study focused on assessing the practical utility of TLRS under various formulation conditions, rather than performing a full validation in accordance with ICH Q2(R1) guidelines. Because principal component analysis (PCA) was employed as the primary quantitative approach, traditional regression-based parameters such as limit of detection (LOD) and limit of quantification (LOQ) could not be directly determined. Nonetheless, we estimated the sensitivity of the method using signal-to-noise ratio (S/N)-based evaluations from Raman spectra. Additionally, the clustering clarity and separation

observed in the PCA score plots serve as indirect indicators of the method's reproducibility and discrimination capability. This study did not compare TLRS with PXRD or DSC. A previous report has shown that TLRS provides higher sensitivity for detecting trace crystallinity than conventional techniques.[34] The present study builds upon those findings by exploring the effects of formulation parameters—such as tablet thickness, particle size, and compaction pressure—on the TLRS signal and its reliability. While carbamazepine was used as a model API, the TLRS approach is broadly applicable, and we plan to extend its use to other pharmaceutical compounds. Furthermore, future work will incorporate regression-based models such as partial least squares regression (PLSR) to enable full quantitative validation. However, it should be noted that the applicability of TLRS strongly depends on the presence of distinct lattice vibrational peaks associated with the crystalline structure of the target API and their minimal overlap or interference from excipient bands. These conditions are essential for reliable differentiation of crystalline and amorphous phases and should be carefully verified when applying TLRS to other formulations. From a practical standpoint, TLRS performance can be optimized by controlling key factors identified in this study. Selecting tablet thickness near the optimal range (approximately 2–4 mm) ensures efficient light transmission, while avoiding excessive compaction prevents signal attenuation. Using smaller particle sizes (≤212 μm) improves spectral reproducibility and semi-quantitative accuracy. These findings provide useful guidance for applying TLRS in pharmaceutical quality control.

Conclusions

This study evaluated the feasibility of using TLRS for the quantitative analysis of crystalline content in amorphous pharmaceutical tablets. TLRS enables nondestructive and sensitive detection of residual crystals in intact tablets, which is critical for maintaining formulation stability and ensuring product quality. Although the present findings were obtained using carbamazepine as a model API, the applicability of TLRS is influenced by the spectral characteristics of each compound and excipient. We systematically evaluated key formulation and measurement parameters including tablet thickness, compaction pressure, particle size, and laser intensity. Each parameter influenced Raman signal intensity and quantification performance. Notably, an optimal tablet thickness was required to maximize signal in the transmission mode, and smaller particle sizes produced more reproducible spectra and enhanced quantification accuracy. Multivariate analysis further confirmed that spectral data could effectively differentiate samples with varying crystalline contents, particularly when broader spectral regions were utilized. Compared with conventional solid-state techniques, TLRS provides a unique combination of deep sampling capability, spectral sensitivity in the lattice mode region, and nondestructive assessment of bulk tablet composition. These advantages indicate that TLRS is a promising analytical tool for quality control and stability testing in the development of amorphous solid dosage forms. The nondestructive quantification of low crystallinity levels offers valuable insights during formulation development, process monitoring, and quality assurance. This capability may facilitate real-time monitoring of recrystallization during manufacturing and support control strategies for formulations prone to polymorphic transitions. Nevertheless, future studies should aim to expanding the technique to a wider range of APIs and integrating it into in-line or at-line manufacturing workflows.

Experimental

Materials

CBZ (Form III) was obtained from Tokyo Chemical Industry Co., Ltd (Tokyo, Japan) for use as the model drug. Microcrystalline cellulose (MCC, Theolus® UF-702) was kindly provided by Asahi Kasei Corporation (Tokyo, Japan) for use as the excipient. The amorphous form of CBZ (CBZ_amo) was prepared using the melt-quenching method, 41 in which CBZ Form III was heated until melted and then rapidly cooled. The identity and physical state of both CBZ Form III and CBZ_amo were confirmed using LRS and PXRD. Fig. 1 presents the chemical structures of the compounds, and Fig. 2 shows the LRS and PXRD results.

Tablet preparation conditions

Tablets were prepared with CBZ Form III contents ranging from 0 to 30% (w/w) blended with amorphous CBZ (CBZ_amo) and MCC at a fixed excipient-to-drug ratio of 0.3 (w/w). The amorphous form of CBZ was obtained by heating CBZ Form III to 190 °C and rapidly cooling it to room temperature on an aluminum plate. The mixtures were homogenized for 30 s using a vortex mixer. The blended powders were directly compressed into tablets using a manual tablet press equipped with an 8 mm diameter die (Riken Instruments Co., Ltd, Tokyo, Japan). Tablet weights ranged from 60 to 200 mg, and compaction pressures of 10, 20, or 30 MPa were applied for 10 s. Particle size classification of CBZ Form III and CBZ_amo was performed using sieves with mesh openings of 212, 100, and <100 μm.

Raman spectroscopy

Low-frequency Raman spectra were obtained using a THz Raman probe system (MarqMetrix Inc., Monrovia, CA, USA) equipped with an 808 nm laser and the RAMAN ALL-IN-ONE detector unit from the same manufacturer. All measurements were conducted under dark conditions to minimize noise. Furthermore, the exposure time per spectrum was set to 1 s, and each sample was measured with three spectral integrations.

Spectral analysis

The collected Raman spectra were subjected to principal component analysis (PCA) using JMP PRO 16.0 software (SAS Institute Inc., Cary, NC, USA). Before conducting multivariate analysis, spectral preprocessing was performed by standard normal variate transformation using Grams/AI 8.0 software

(Thermo Fisher Scientific Inc., MA, USA). PCA was used to explore clustering behavior and investigate the influence of formulation variables on the spectral profile.

Author contributions

Reo Kasahara: investigation, methodology, writing – original draft. Motoki Inoue: conceptualization, data curation, formal analysis, funding acquisition, investigation, methodology, project administration, supervision, writing – original draft, writing – review and editing. Toshiro Fukami: resources, writing – review and editing.

Conflicts of interest

There are no conflicts to declare.

Data availability

The data supporting this study have been included in the article.

Acknowledgements

References

1 N. Qiao, M. Li, W. Schlindwein, N. Malek, A. Davies and G. Trappitt, *Int. J. Pharm.*, 2011, **419**, 1–11.
2 S. Aitipamula, R. Banerjee, A. K. Bansal, K. Biradha, M. L. Cheney, A. R. Choudhury, G. R. Desiraju, A. G. Dikundwar, R. Dubey, N. Duggirala, P. P. Ghogale, S. Ghosh, P. K. Goswami, N. R. Goud, R. R. K. R. Jetti, P. Karpinski, P. Kaushik, D. Kumar, V. Kumar, B. Moulton, A. Mukherjee, G. Mukherjee, A. S. Myerson, V. Puri, A. Ramanan, T. Rajamannar, C. M. Reddy, N. Rodriguez-Hornedo, R. D. Rogers, T. N. G. Row, P. Sanphui, N. Shan, G. Shete, A. Singh, C. C. Sun, J. A. Swift, R. Thaimattam, T. S. Thakur, R. Kumar Thaper, S. P. Thomas, S. Tothadi, V. R. Vangala, N. Variankaval, P. Vishweshwar, D. R. Weyna and M. J. Zaworotko, *Cryst. Growth Des.*, 2012, **12**, 2147–2152.
3 P. Vishweshwar, J. A. McMahon, J. A. Bis and M. J. Zaworotko, *J. Pharm. Sci.*, 2006, **95**, 499–516.
4 K.-I. Izutsu, T. Koide, N. Takata, Y. Ikeda, M. Ono, M. Inoue, T. Fukami and E. Yonemochi, *Chem. Pharm. Bull.*, 2016, **64**, 1421–1430.
5 M. Qin, G. Ye, J. Xin, M. Li, X. Sui, Y. Sun, Q. Fu and Z. He, *Int. J. Pharm.*, 2023, **636**, 122793.
6 J.-I. Jinno, N. Kamada, M. Miyake, K. Yamada, T. Mukai, M. Odomi, H. Toguchi, G. G. Liversidge, K. Higaki and T. Kimura, *J. Controlled Release*, 2006, **111**, 56–64.
7 S. B. Murdande, M. J. Pikal, R. M. Shanker and R. H. Bogner, *J. Pharm. Sci.*, 2010, **99**, 1254–1264.
8 S. B. Murdande, M. J. Pikal, R. M. Shanker and R. H. Bogner, *Pharm. Res.*, 2010, **27**, 2704–2714.
9 N. J. Babu and A. Nangia, *Cryst. Growth Des.*, 2011, **11**, 2662–2679.
10 K. Kawakami, *J. Pharm. Sci.*, 2009, **98**, 2875–2885.
11 K. A. Graeser, J. E. Patterson, J. A. Zeitler, K. C. Gordon and T. Rades, *Eur. J. Pharm. Sci.*, 2009, **37**, 492–498.
12 P. T. Mah, S. J. Fraser, M. E. Reish, T. Rades, K. C. Gordon and C. J. Strachan, *Vib. Spectrosc.*, 2015, **77**, 10–16.
13 J. Griffen, A. Owen and P. Matousek, *J. Pharm. Biomed. Anal.*, 2015, **115**, 277–282.
14 B. Shah, V. K. Kakumanu and A. K. Bansal, *J. Pharm. Sci.*, 2006, **95**, 1641–1665.
15 N. Chieng, T. Rades and J. Aaltonen, *J. Pharm. Biomed. Anal.*, 2011, **55**, 618–644.
16 G. A. Stephenson, R. A. Forbes and S. M. Reutzel-Edens, *Adv. Drug Delivery Rev.*, 2001, **48**, 67–90.
17 X. Chen, S. Bates and K. R. Morris, *J. Pharm. Biomed. Anal.*, 2001, **26**, 63–72.
18 M. K. Hatipoglu, Y. Zaker, D. R. Willett, N. Gupta, J. D. Rodriguez, S. Patankar, P. Capella and H. Yilmaz, *Anal. Chem.*, 2023, **95**, 15325–15332.
19 S. Roy, B. Chamberlin and A. J. Matzger, *Org. Process Res. Dev.*, 2013, **17**, 976–980.
20 S. Hubert, S. Briancon, A. Hedoux, Y. Guinet, L. Paccou, H. Fessi and F. Puel, *Int. J. Pharm.*, 2011, **420**, 76–83.
21 L. Liang, J. Zhang, B. G. Sumpter, Q.-H. Tan, P.-H. Tan and V. Meunier, *ACS Nano*, 2017, **11**, 11777–11802.
22 B. S. Kalanoor, M. Ronen, Z. Oren, D. Gerber and Y. R. Tischler, *ACS Omega*, 2017, **2**, 1232–1240.
23 K. N. Woods, J. Pfeffer, A. Dutta and J. Klein-Seetharaman, *Sci. Rep.*, 2016, **6**, 37290.
24 H. Nie, G. Klinzing and W. Xu, *Int. J. Pharm.*, 2022, **617**, 121608.
25 P. J. Larkin, J. Wasylyk and M. Raglione, *Appl. Spectrosc.*, 2015, **69**, 1217–1228.
26 K. Shin and H. Chung, *Analyst*, 2013, **138**, 3335–3346.
27 J. Johansson, S. Pettersson and S. Folestad, *J. Pharm. Biomed. Anal.*, 2005, **39**, 510–516.
28 M. Kim, H. Chung, Y. Woo and M. Kemper, *Anal. Chim. Acta*, 2006, **579**, 209–216.
29 M. V. Schulmerich, W. F. Finney, R. A. Fredricks and M. D. Morris, *Appl. Spectrosc.*, 2006, **60**, 109–114.
30 P. Matousek and A. W. Parker, *Appl. Spectrosc.*, 2006, **60**, 1353–1357.
31 P. Matousek and A. W. Parker, *J. Raman Spectrosc.*, 2007, **38**, 563–567.
32 M. Inoue, T. Osada, H. Hisada, T. Koide, T. Fukami, A. Roy, J. Carriere and R. Heyler, *Anal. Chem.*, 2019, **91**, 13427–13432.
33 M. Inoue, T. Osada, H. Hisada, T. Koide, T. Fukami, A. Roy and J. Carriere, *J. Pharm. Sci.*, 2023, **112**, 225–229.

34 M. Inoue, H. Hisada, T. Koide, T. Fukami, A. Roy, J. Carriere and R. Heyler, *Anal. Chem.*, 2019, **91**, 1997–2003.

35 M. Inoue, T. Akiyama and T. Fukami, *Analyst*, 2025, **150**, 2574–2579.

36 A. Sparén, M. Hartman, M. Fransson, J. Johansson and O. Svensson, *Appl. Spectrosc.*, 2015, **69**, 580–589.

37 N. Everall, I. Priestnall, P. Dallin, J. Andrews, I. Lewis, K. Davis, H. Owen and M. W. George, *Appl. Spectrosc.*, 2010, **64**, 476–484.

38 H. Fael and A. L. Demirel, *Int. J. Pharm.*, 2020, **581**, 119284.

39 N. Townshend, A. Nordon, D. Littlejohn, J. Andrews and P. Dallin, *Anal. Chem.*, 2012, **84**, 4665–4670.

40 S. Gupta, B. Igne, T. Omar, A. D. Román-Ospino, D. Hausner and F. Muzzio, *Int. J. Pharm.*, 2022, **624**, 122052.

41 S. Virtanen, O. Antikainen and J. Yliruusi, *Int. J. Pharm.*, 2008, **360**, 40–46.

42 J. Kim, Y. Kim and H. Chung, *Talanta*, 2011, **83**, 879–884.